Bio-Design and Manufacturing (2023) 6:38–50
https://doi.org/10.1007/s42242-022-00215-1

RESEARCH ARTICLE

Junction matters in hydraulic circuit bio-design of microfluidics

Yao Lin[1] · Dongliang He[1] · Zerui Wu[1] · Yurou Yao[1] · Zhanhao Zhang[2] · Yuheng Qiu[1] · Shan Wei[1] · Guangzhu Shang[1] · Xingyue Lei[1] · Ping Wu[3] · Weiping Ding[4] · Liqun He[1]

Received: 23 May 2022 / Accepted: 18 September 2022 / Published online: 11 November 2022

Abstract

Microfluidic channels are at micrometer scales; thus, their fluid flows are laminar, resulting in the linear dependence of pressure drop on flow rate in the length of the channel. The ratio of the pressure drop to flow rate, referred to as resistance, depends on channel size and dynamic viscosity. Usually, a microfluidic chip is analogous to an electric circuit in design, but the design is adjusted to optimize channel size. However, whereas voltage loss is negligible at the nodes of an electric circuit, hydraulic pressure drops at the nodes of microfluidic chips by a magnitude are comparable to the pressure drops in the straight channels. Here, we prove by experiment that one must fully consider the pressure drops at nodes so as to accurately design a precise microfluidic chip. In the process, we numerically calculated the pressure drops at hydraulic nodes and list their resistances in the range of flows as concerned. We resorted to machine learning to fit the calculated results for complex junctions. Finally, we obtained a library of node resistances for common junctions and used them to design three established chips that work for single-cell analysis and for precision allocation of solutes (in gradient and averaging concentration microfluidic networks). Endothelial cells were stimulated by generating concentrations of adriamycin hydrochloride from the last two microfluidic networks, and we analyzed the response of endothelial cells. The results indicate that consideration of junction resistances in design calculation brings experimental results closer to the design values than usual. This approach may therefore contribute to providing a platform for the precise design of organ chips.

Graphic abstract

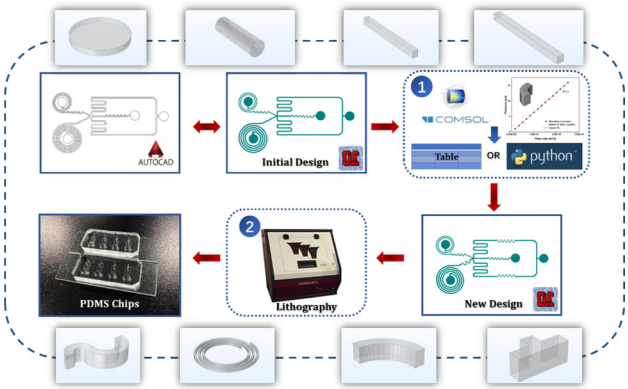

Keywords Junctions · Hydraulics · Microfluidic chip design

Yao Lin and Dongliang He have contributed equally to this work.

✉ Weiping Ding
wpdings@ustc.edu.cn

✉ Liqun He
heliqun@ustc.edu.cn

[1] Department of Thermal Science and Energy Engineering, University of Science and Technology of China, Hefei 230027, China

[2] School of Chemistry and Materials Science, University of Science and Technology of China, Hefei 230027, China

[3] GeneMind Biosciences Company Limited, Shenzhen 518023, China

[4] Department of Electronic Engineering and Information Science, University of Science and Technology of China, Hefei 230027, China

Introduction

Since its advent [1], microfluidics has been used to reduce the demand of chemistry and biology systems in terms of size, labor, and time, such that experiments could be carried out more rapidly with fewer chemicals than usual. Nowadays, microfluidics has grown far beyond this purpose, and many novel applications have been found, for instance, wearable sensors [2–5], single-cell analyses [6], digital droplet polymerase chain reaction (PCR) [7], biomedical particles [8, 9], single-molecule screening [10], organics on chips [11] and functional polymeric materials [12]. Accordingly, professional people in several fields like doctors and research scientists are turning to microfluidics. In such circumstances, one must have a suitable protocol to design precise, functional microfluidics [13]. It is effective for one to tune the real fluid flow with valves at a running time [14]; however, active controls require more complex design and fabrication, as well as development of algorithms and tools to monitor specific sensors. So, it is valuable to design a microfluidics chip with a geometry-mediated method as much as possible. People can design microfluidics chips as shown in Table 1. With the aid of numerical solutions to fluid dynamics, or other tools such as rapid design for concentration gradient generation [15–17], a web-based interactive tool for designing microfluidic chips [18], paper-based microfluidics chips [19], and even artificial intelligence (AI)-based methods [20], people can obtain concentration gradient circuit and microfluidic mixer design. Besides these methods for specific applications [21, 22], the hydraulic circuit method proposed here would serve for broader applications, if the resistances of microfluidic channels could be precisely modeled.

It is well known that the hydrodynamics in microfluidics lies in the laminar regime, and the shear stress of walls is dominant over the fluid inertia. Therefore, it is hard for cross-currents to occur in microfluidics, a fact that makes it possible to mathematically reduce their hydrodynamics to an effective electric circuit. As a result, one can solve the pressures at node and flow rates in the channel simultaneously, as in an electric circuit [23]. This means that the design of a microfluidic system becomes a task of laying out the network of the hydraulic resistor. In other words, those designing a microfluidic system turn their attention from solving the hydrodynamics to calculating the matrix of a resistor circuit [24–26]. Therefore, various methods available for the electric circuit will help in designing a microfluidic chip. Although the similarity of a hydraulic circuit to an electric circuit is of great help, electricity is not exactly the same as fluid flow, and the analogy seems to work well only in symmetrical hydraulic circuits [27–30]. What challenges the analogy is the energy cost at the node. In an electric circuit, there is a unique voltage at a junction, but there is an obvious loss in hydraulic pressure across a junction in a hydraulic circuit. That is, the energy cost due to dividing or mixing fluid flow is noticeable as compared to that in straight channels [28, 31]. For a symmetric configuration, one can allocate the energy loss evenly to branches of a junction in the upstream/downstream as long as their resistances are kept as equal as possible at the design stage. However, when it comes to asymmetrical structures [32], one must know the precise allocation of pressure loss to individual branches.

In the framework of hydraulic circuit design, the allocation of pressure loss at a junction to its branches has to be considered after calculation of hydraulic resistances and be done in piping systems as well [33–35]. As demonstrated below, resistances at junctions in microfluidics, for instance, at the elbow, tee, cross, and input/output, are comparable to those in the channels [36]. They do influence flow rates downstream, as well as chemicals or droplets for later reactions [37]. In order to take the junctions into account in microfluidic design, one has to prepare a list of junction resistances for immediate use [27, 28, 31], for instance, at the elbow, tee, snaked tube, and helical tube. A provided junction list particularly benefits people from various backgrounds [38] who hope to streamline a design without the need for any knowledge of fluid dynamics [39, 40].

Cell function is regulated by a variety of chemical signals in the microenvironment [41], such as hormones, cell metabolites, and drugs. Understanding the effects of these chemicals on cells may help in developing controlled microenvironments in which the desired cellular response is produced. The dose–response relationship is an important index to evaluate cellular response in cell-chemical stimulation. Such experiments usually involve applying chemical stimuli to cells at gradient concentrations, and observing cell response to various intensities of stimuli at a given time. Therefore, it is very important to generate the gradient concentration with simultaneous and accurate control [32]. Clearly, accurate design of microfluidic chips is a challenge. In this work, we studied the junction resistances of L-junctions, T-junctions, snaked junctions, and helix junctions, and built a library. We gave the process of design and fabrication of the microfluidic chips. Through single-cell analysis, we validated the reliability of the design method for precision allocation of concentration in microfluidic chips. Using this method, we were able to develop microfluidic chips with highly precise allocation of solutes for the study of cell-chemical stimulation. We investigated the effect of concentration formation from the microfluidic chips on endothelial cell culture, which provided beneficial insights into drug screening with microfluidic chips at the cellular level.

Table 1 Microfluidic chip-design strategy

Title	Purpose	Method	Tool	Reference
Random design of microfluidics	Concentration gradient circuit design	Software of web version	MATLAB program; COMSOL Multiphysics; MySQL database	[15]
Finding the optimal design of a passive microfluidic mixer	Microfluidic mixer design	FEA and algorithm	COMSOL Multiphysics; Algorithm II (NSGAII)12	[16]
Predicting the fluid behavior of random microfluidic mixers using convolutional neural networks	Microfluidic mixer design	Machine learning-CNN	CNN	[17]
A correct-by-construction design and programming approach for open paper-based digital microfluidics	Paper-based digital microfluidics	OPB-DMF platform	Hardware and software tools	[21]
Toward microfluidic design automation: a new system simulation toolkit for the in silico evaluation of droplet-based lab-on-a-chip systems	Modeling droplet traffic and processing	Toolkit	Algorithm based on the Kirchhoff laws	[22]
Junction matters in hydraulic circuit bio-design of microfluidics	2D/3D microfluidics systems	Machine learning-Sklearn package	Python program; COMSOL Multiphysics	This work

Materials and methods

Fabrication of the microfluidic chips

Microfluidic chips were made of polydimethylsiloxane (PDMS) as usual, and the patterns were written into the layers of photoresist (Micro Chem, SU-8 2050) by a desktop maskless laser direct writing lithography machine (MicroWriter ML® 3, Durham Magneto Optics, UK) after the patterns had been finished by the drawing software (CleWin 5.2 Layout Editor). The height of all layers was 120 μm. The photoresist layers were coated by a Spin Coater (EZ4). After cleaning with the developer (Micro Chem, SU-8), a clean pattern of photoresist was obtained on the silicon wafer. Then, a mixture at a mass ratio of 10:1 of PDMS (Sylgard®184 Silicone Elastomer) and PDMS Curing Agent (Sylgard®184 Silicone Elastomer Curing Agent) was poured over the patterns. After bubble removal in a vacuum and solidification in an oven (DB-2A, China), the PDMS film was removed and then cleaned with a plasma cleaning machine (PDC-MG, China). Then, the PDMS film was bonded on a slide that had been polished by plasma. Unless otherwise stated, all chemical reagents used in this study were of analytical grade; ultrapure water was prepared with a pure water system (Mill-Q Advantage A10).

Optical observation platform

We set up a custom system to observe the performance of a microfluidics chip (Fig. 1). There were three entries into the chip for single-cell analysis, two of which served as the two helical channels and were filled with red and green dye solutions. The last entry was fed with a blue dye solution which simulated oil carrier. The whole chip worked under negative pressure; that is, an injected syringe (LSP02-2B Dual Channels Syringe Pump) was connected to the exit and worked in the pull mode. The typical flow rate was 40 μL/min. In the experiment, we loaded 750 μL of dye (Rhodamine B, Shanghai, China) in a polyethylene tube (BB31695-PE/2) and 25 mL of deionized water in a storage bottle (Scientific Commodities Inc.). With regard to precise allocation of solutes, the whole chip also worked under negative pressure, achieved by a syringe in pull mode at the exit.

Image recordings

For image recording, we used dyes to reveal the results of the design. As stated above, the fluid flows as in a strong laminar regime, and the dyes in two parallel streams did not mix with each other across their streamlines by convection. Therefore, their concentrations in the mixture along the exit channel

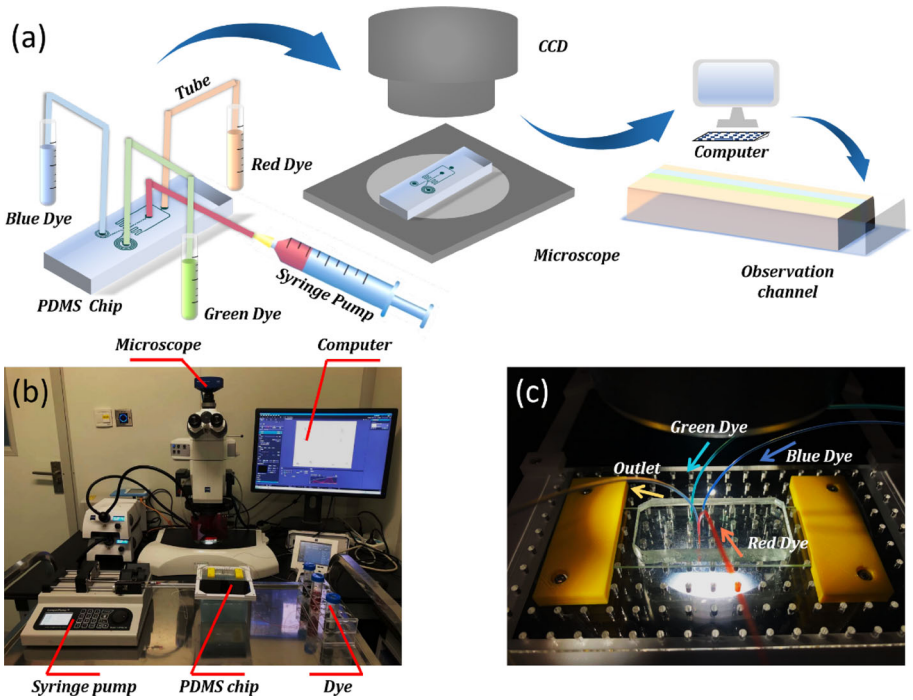

Fig. 1 The laminar flow experimental system: **a** schematic diagram, **b** physical diagram, **c** the microfluidic chip under a microscope

could be measured directly by their widths [42–44]. We set observation windows over each exit channel and recorded the corresponding width; still images were taken with a camera (Axiocam 506 color) under a stereoscopic microscope (Zeiss V16, Germany). Images were acquired using the built-in software (CellSens Dimension Software with an accuracy of 0.01 μm). Image analysis and post-processing were performed with ImageJ software.

Cell seeding and staining

When the cells proliferated to a monolayer discontinuous state in the culture flask, the medium was removed and treated with 2.5% trypsin (Biological Industries) for 2 min. After the cells were re-suspended in fresh medium, the cell suspension was centrifuged at 1600 r/min for 5 min. Using a cell-counting plate to estimate the number of cells, we adjusted the cell suspension density to 10^6 cells/mL. Different gradients of adriamycin hydrochloride (Pharmacia-Upjohn, Milan, Italy) with different gradients generated by the microfluidic chip were introduced into cultured cells, and transferred to an incubator (37 °C and 5% CO_2) for 6 h. The fluorescent dye solution was prepared with phosphate balanced solution (PBS). The dye ratio in the AO/EB (acridine orange and ethidium bromide) solution was 2.5 μg/L. In addition, the adriamycin hydrochloride stimulated group and the blank control group had fluorescent dye solution added to mark cell survival status. After 15 min of dye labeling, the cells were observed under a fluorescence microscope. Cell fluorescence images were analyzed with ImageJ software, and cell death was determined by color. In addition, we calculated the proportion of living cells. The reagents used were all analytical grade, and the solutions were prepared with sterile secondary distilled water.

Theory and model

In microfluidics, the fluid flow in a straight channel is mathematically reduced to Poisson flow, resulting in analytic forms of resistances. In our study on fluid flow through junctions, we had to resort to numerical solutions to Navier–Stokes equations to obtain the resistances. The results are expressed here in a form that meets the hydraulic design needs. Generally, what we do includes two kinds of tasks: (1) creating modules, and (2) designing a system. In the hydraulic view, a microfluidics system is equivalent to a directed graph for which both the edges and nodes are to be set. Edges are straight channels that are transformed to edge resistors, while nodes are junctions of the resistor to be modeled here. With the advent of new applications, new junctions will appear, and we will be able to obtain their resistances on demand.

Junction resistances

The resistance of junctions was solved numerically because junctions can have a variety of shapes based on the requirements. To set a reference for numerical calculation, we began with a model for the rectangle of a straight channel. By carefully tuning parameters, we achieved the numerical results closest to the straight channel's exact value (Extended data 1

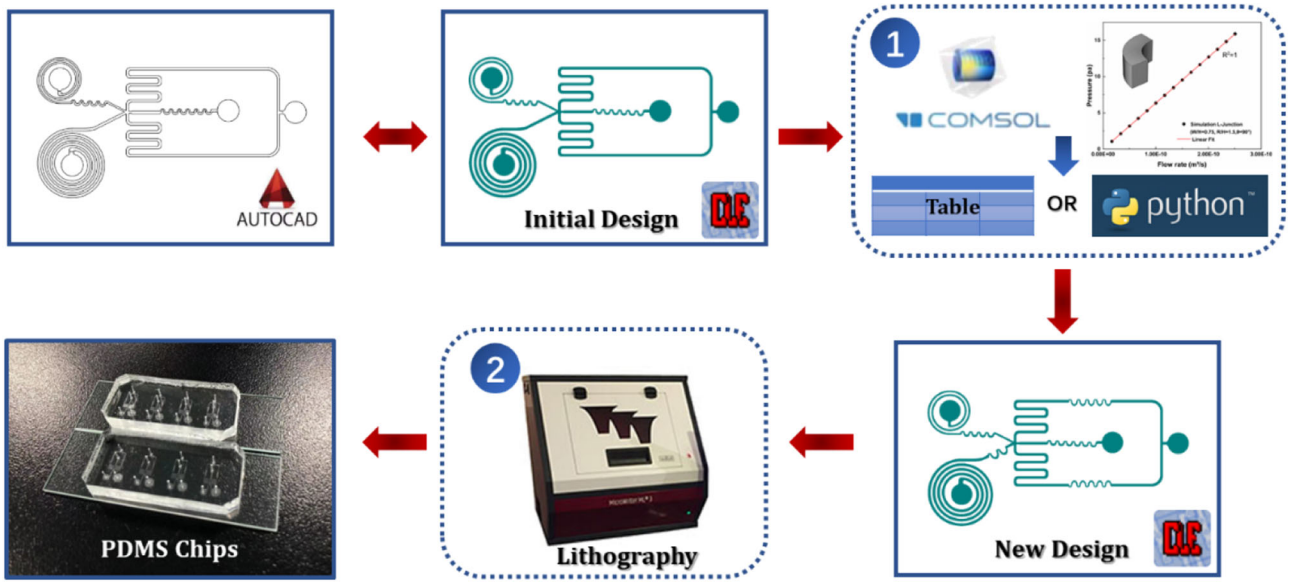

Fig. 2 Design and fabrication process diagram for the microfluidic chips. Step 1: using the Sklearn package in Tables/Python (Extended data 2 and 3 in Supplementary Information) to obtain the new designs. Step 2: lithography

in Supplementary Information), and then we kept these settings for calculation of all junctions, including L-junctions, T-junctions, snaked junctions, and helix junctions. The geometrical models of these junctions were first created with AutoCAD (Extended data 2 in Supplementary Information), and then imported into COMSOL. In the calculation, the height of the channel was set as 120 μm, and the laminar flow module was chosen. The channel inlet was set with a flow rate varying between 1 and 15 μL/min in steps of 1 μL/min. The channel outlet was set to a pressure of zero. Geometry meshing was carefully tuned to balance the length of running time and accuracy of results. For example, in the case of the L-junction (W/H=0.75, R/H=1.5, θ=90°) (Fig. 2), we set a free quadrilateral grid over the cross section of the entry, and then the meshed cross section swept the whole junction.

We obtained the pressure at entry for the range of flow rates commonly used in practice and plotted these values against their associated flow rates. The pressures were fitted with a linear model, and the resultant slope (R) represents the hydraulic resistance of a junction. The resistances of all junctions were obtained with the same settings (Extended data 2 in Supplementary Information). We resorted to machine learning to fit the complex junctions that had many parameters that defined their resistance. Specifically, we used the Sklearn package in Python to train the data and predict the complex junctions resistance, as coded in Extended data 3 (Supplementary Information). Finally, we tabulated a minimal set of modular resistances for design purposes, including channels and junctions, in Table 2. The process diagram of the design and fabrication of the microfluidic chips is shown in Fig. 2. There were two main steps in completing this modular design process. First, we had to have our predesigned program drawn in the CleWin software. After that, we started the hydraulic calculation with the help of tables and a Python program (Extended data 2 and Extended data 3 in Supplementary Information), and thus obtained the target design. In step 2, the new design was fabricated by lithography. This process was fast and accurate and is intended to prevent the need for adjustments after fabrication of the microfluidic chips.

Results and discussion

Validation of the flow-focusing Drop-seq platform

As shown in Fig. 3, there are two spiral channels to focus cells and beads, respectively, with the aid of Dean flow, and the resultant flow-focusing Drop-seq platform serves for single-cell analysis. There are three inlets (A, B, and C) and one outlet (D). Entry A is open for oil carriers, and the suspensions of beads and cells flow into entries B and C, respectively. After cells and beads have been focused separately in their own channels, they meet at the junction and then form one stream at a five-branched junction before meeting with an oil carrier that comes in from two sides. The stream is then squeezed into droplets. Finally, there are a few positive droplets that contain only one cell and one bead at

Table 2 Resistors and nodes for microfluidics

Class	Name	Mark	AutoCAD Model	COMSOL Model	Resistance Calculation	*R* Calculation
Port	Port	R_P			—	—
Line	Rectangle Pipe	R_{RP}			$\Delta p = R_{RP}Q$	$R_{RP} = \frac{12\mu L}{WH^3}[1 - \frac{192H}{\pi^5 W}\tanh(\frac{\pi W}{2H})]^{-1}$
	Square Pipe	R_{SP}	—		$\Delta p = R_{SP}Q$	$R_{SP} = \frac{12\mu L}{W^4}[1 - \frac{192}{\pi^5}\tanh(\frac{\pi}{2})]^{-1}$
	Circular Pipe	R_{CP}	—		$\Delta p = R_{CP}Q$	$R_{CP} = \frac{8\mu}{\pi r^4}$
Resistor	L-Junction	R_L		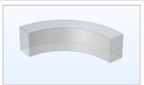	$\Delta p = R_L Q$	Table S2/L-Junction Sklearn.model
	T-Junction	R_{T-I} R_{T-II}			$\Delta p = R_T Q$	Table S3 and Table S4/T-Junction Sklearn.model
	Snaked	R_S			$\Delta p = R_S Q$	Table S5/Snaked Sklearn.model
	Helix	R_H			$\Delta p = R_H Q$	Table S6/Helix Sklearn.model

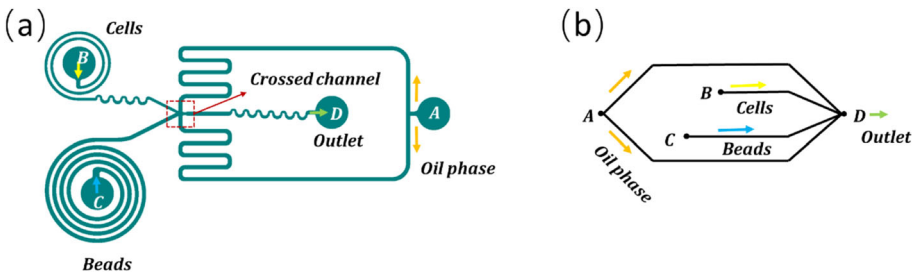

Fig. 3 Flow-focusing Drop-seq platform: **a** schematic diagram, **b** equivalent hydraulic circuit. The ports include inlets (A, B, and C) and outlet (D). There are four branches. The branches through oil are symmetrical from inlet A to outlet D, and are, respectively, denoted as A_1D and A_2D. The branch through cells from inlet B to outlet D is denoted as BD. The branch through beads from inlet C to outlet D is denoted as CD

the same time, and most of the droplets are negative, including empty droplets and droplets with multiple beads or cells. The ratio of the number of droplets with one bead and one cell to the total number of droplets defines the efficiency of the chip. Obviously, the two spiral channels are asymmetric around the junction. In order for them to work under negative pressure as expected, one must know the precise resistances of all branches against design flow rates. Only in this way can a highly efficient chip be designed.

As usual, the hydraulic resistance of one branch in microfluidic device design is determined only by the channel, not by the junction. In this flow-focusing Drop-seq chip, the length ratio of the four branches is L_{A_1D}:L_{BD}:L_{CD}:L_{A_2D}=7.58:15.17:7.05:7.58, and thus, the design resistances of both branch A_1D and branch A_2D should be 1.06×10^{12} (Pa·s)/m^3. The design resistance of branch BD is 6.27×10^{12} (Pa·s)/m^3, and that of branch CD is 3.88×10^{12} (Pa·s)/m^3. To see the result of the design, we fed three colored solutions into the experimental system as described above, and observed the results at the exit (Fig. 1). The four colored streams are meant to run in parallel in the exit channel and their width ratio should be 1:1:1:1. However, the observed values (Fig. 4a3) were 48.72, 9.98, 13.04, and 47.65 μm (4.88:1:1.31:4.77). That is, the real operating flow rates were different from the design values. We attribute

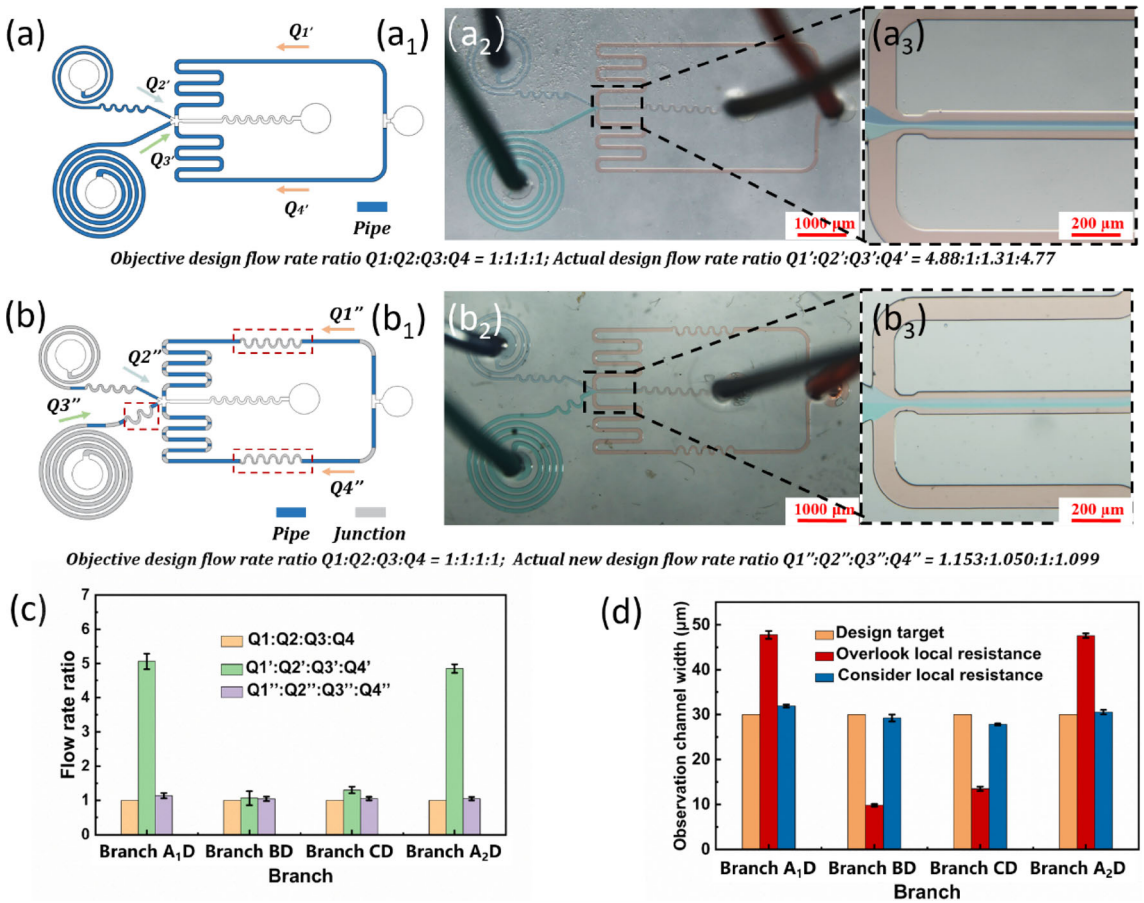

Fig. 4 The role of junction resistances in the design. $\mathbf{a_1}$ Microchips were divided into resistance zones by considering junctions. $\mathbf{a_2}$ Observation of the exit channel in experiments on the primary chip. The scale bar denotes 1000 μm. $\mathbf{a_3}$ Four streams in parallel in the exit channel of the primary chip. The scale bar denotes 200 μm. $\mathbf{b_1}$ New design of the microchip incorporating junction resistances. $\mathbf{b_2}$ Observation of the exit channel in experiments on the improved chip. The scale bar denotes 1000 μm. $\mathbf{b_3}$ Four streams in parallel in the exit channel of the improved chip. The scale bar denotes 200 μm. **c** The flow rate ratio of four branches. Objective design flow rate ratio (Q1:Q2:Q3:Q4); actual design flow rate ratio (Q1':Q2':Q3':Q4'); actual new design flow rate ratio (Q1":Q2":Q3":Q4"). **d** Observed widths of the four streams in the exit channel

this deviation to the fact that people ignored junction resistances, and we redesigned the chip taking these into account (Extended data 4 in Supplementary Information). In the process of the new design (Fig. 4b1), we considered junction resistances when keeping the ratio 1:1:1:1, and then repeated the above experiment. The observed widths of the four colors were 32.07, 29.20, 27.81, and 30.59 μm; these resulted in a ratio of 1.153:1.050:1:1.099 (Figs. 4b2 and 4b3), indicating that the flow rates were very close to the real values in the design once the junction resistances were taken into consideration (Figs. 4c and 4d).

Validation of the concentration gradient circuit

To further highlight the importance of junction resistances, we designed a mixing circuit to create a concentration gradient at the exit. That is, two or more fluids were fed into the circuit and then several mixtures exited at different ratios, as designed. It was important for us to know the exact hydraulic resistances of all mixing paths at the design stage. As demonstrated below, taking into account the junction resistances will lead to more precisely mixing results.

When subjected to constant pressure, the flow rates in a microfluidics circuit are simply limited by resistances:

$$C_{\text{Design}} = \frac{Q_1}{Q_1 + Q_2} C_1 + \frac{Q_2}{Q_1 + Q_2} C_2 = \frac{R_2}{R_1 + R_2} C_1 + \frac{R_1}{R_1 + R_2} C_2, \quad (1)$$

where C_{Design} is the target concentration at design, C_1 and C_2 are the concentrations of two input fluids, Q_1 and Q_2 are their flow rates, and R_1 and R_2 are their resistances.

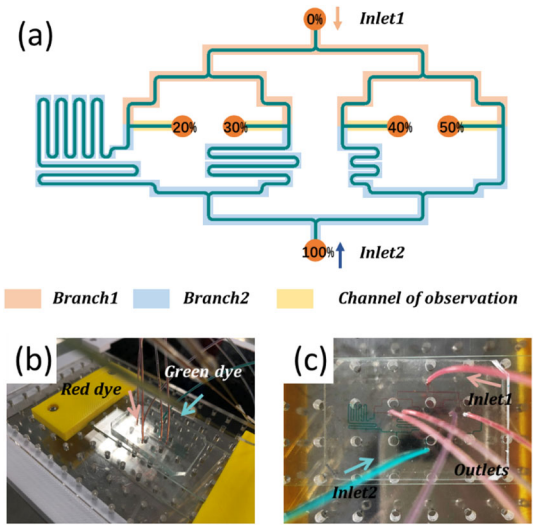

Fig. 5 Concentration gradient chip: **a** schematic diagram, **b** physical diagram, **c** the microfluidic chip under a microscope. Entries and exits are indicated by solid circles

We designed this microfluidic chip for high-precision mixing, and the detailed design process can be seen in Extended data 5 (Supplementary Information). The aim of the circuit was to obtain mixtures (μg/mL) of 20%, 30%, 40%, and 50% of two input solutions whose concentrations were set as 0 and 1 for convenience. The two entrances were placed at opposite ends of the chip, and then each input was divided into four branches. Finally, they met at exits along the central line. Entries and exits are indicated as the solid circles in Fig. 5a. The four branches of inlet 1 had the same flow resistance (21.62×10^{11} (Pa·s)/m^3), while the four branches of inlet 2 were designed with varying resistances, resulting in different mixing ratios of flow rates. As stated above, the strong laminar flow makes it possible for the resultant mixture to be a stream of two parallel fluids. We chose the diffusion happening distance which is far less than the flow distance region as the observation window; therefore, we measured the parallel fluids approximately to simplify the process of calculation. The process of verifying the design was greatly simplified by reading the widths of different colors.

$$m_0 = \frac{W_1}{W_2}, \tag{2}$$

where m_0 is the volumetric mixing ratio of two input fluids in the observation channel, and W_1 and W_2 are the observed widths of two input fluids. W_1 and W_2 can be obtained by image processing with ImageJ.

In our experiment, we placed the observation channel below a camera on the microscope, which was used to record the widths. The input fluids were colored with two dyes. The syringe pump operated in the pulling mode, and the microfluidics worked under negative pressure. Their volume mixing ratios (m_0) are known at the design stage, as given by the resistance values of Branch1 and Branch2. That is,

$$m_0 = \frac{Q_1}{Q_2} = \frac{R_2}{R_1}. \tag{3}$$

All channels are rectangular, and their resistance can be estimated by $R = \frac{12\mu L}{WH^3}\left[1 - \frac{192H}{\pi^5 W}\tanh\frac{\pi W}{2H}\right]^{-1}$, where L, H, and W are the length, height, and width of the channel, respectively, and μ is the viscosity.

The operating results are shown in Figs. 6a–6c. Laminar flow stratification of the two dyes can be seen from the reserved observation channel. By comparing the actual dye volume mixing ratio with the designed one, we found that the actual value was in agreement with the designed value, indicating that an accurate microfluidic chip can be designed after considering local resistance (Fig. 6c).

By an external injection syringe pump, the reagents can be introduced into the chip, which can then generate accurately controllable, continuous, and stable parallel concentration gradients. The endothelial cells were stimulated by generating a gradient concentration of adriamycin hydrochloride, and we analyzed the response of endothelial cells, as shown in Figs. 7a–7c. After 12 h of stimulation, we used the fluorescent dye solutions to show the results. The result (Fig. 7d) showed that our microfluidic chip had high precision due to the design method. This precise microfluidic concentration gradient network can be used to study cell-chemical stimuli and has the potential to become a technological platform for drug screening at the cellular level.

L-junction matters in the concentration distribution network of the microfluidic chip

In practice, fluid flow behavior in curved channels is more complex than in electronic circuits. For example, secondary fluid flow in a curved channel usually increases. Taking the L-junction as an example, we found that the quantity, shape, and size of junctions not only affect the resistances, but also make a difference in the transport and distribution of the mixture concentration. We show the results of numerical calculation for junctions of the same shape and size in Fig. 8. The results for the velocity field are shown in Figs. 8a1, 8a2, 8b1, and 8b2. The results for the concentration field are shown in Figs. 8a3, 8a4, 8b3, and 8b4. We transported the same concentration of substances into the inlet at the initial time (Figs. 8a3 and 8b3). With odd numbers of L-junctions, the substance concentration near the outlet will be different after a period, due to the difference between internal and external routes, as shown in Fig. 8a4. However, with even numbers, there will be no obvious imbalance in substance concentration on the inside and outside of the channel near the outlet, as shown in Fig. 8b4.

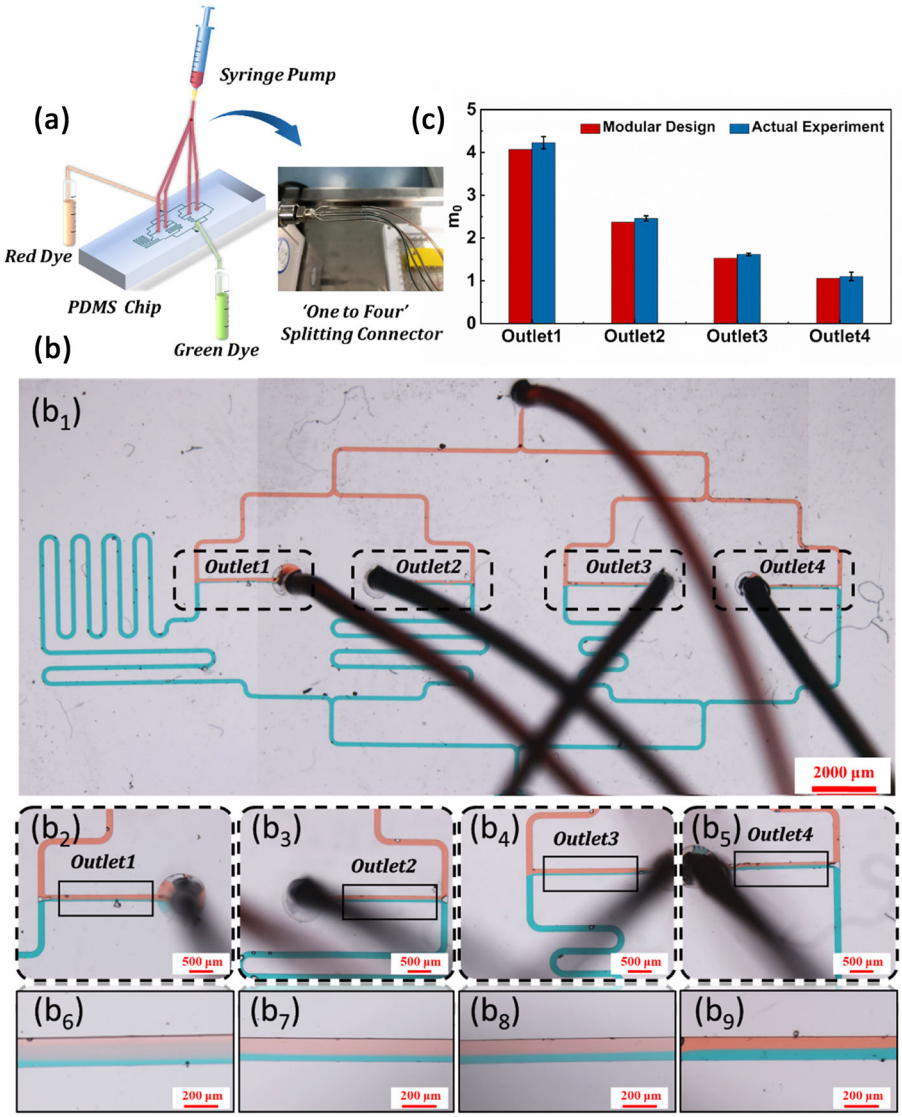

Fig. 6 Observation of mixing results. **a** Schematic diagram of the experimental system. $\mathbf{b_1}$ The whole hydraulic circuit for the concentration gradient. The scale bar denotes 2000 μm. $\mathbf{b_2}$–$\mathbf{b_5}$ The observation window in front of outlets 1, 2, 3, and 4. The scale bars denote 500 μm. $\mathbf{b_6}$–$\mathbf{b_9}$ The widths of two input dyes before outlets 1, 2, 3, and 4. The scale bars denote 200 μm. **c** The volume mixing ratio m_0 at the design stage and in the experiment

Based on the L-junction, we further designed an averaging concentration microfluidic network, as shown in Fig. 9a. The network model has one inlet and eight outlets. It is assumed that the eight outlets have the same concentration after stable operation. Based on the symmetric and asymmetric differences in the layout of junctions, if expectations are to be met, the L-junctions should have the same size and the number of them should be even. From the numerical calculation results (Fig. 9b), we can see the synchronization of the concentration distribution at several different times.

We are more concerned about the concentration distribution in the eight outlets. Figure 9d shows the average concentration of each outlet at different times. It can be seen that the average concentrations from the eight outlets were almost the same. In Fig. 9e, we can see that the average concentration changes of each outlet have almost the same change trend and that the results at different times are very close. We also conducted an experiment to stimulate the endothelial cells by generating concentrations of adriamycin hydrochloride from the averaging concentration microfluidic network (Fig. 9c). From Fig. 9f, we see that the same response was obtained from the cells, which further validates our design method's accuracy. Therefore, paying attention to the important role of junctions in the microfluidic network effectively helped us achieve the establishment of a multi-functional microfluidic network. As in the "one to eight" concentration network, we simply made sure that the L-junction had a reasonable shape and size and that there was an appropriate number of junctions. We believe that this network will be beneficial in many situations in biology and chemistry.

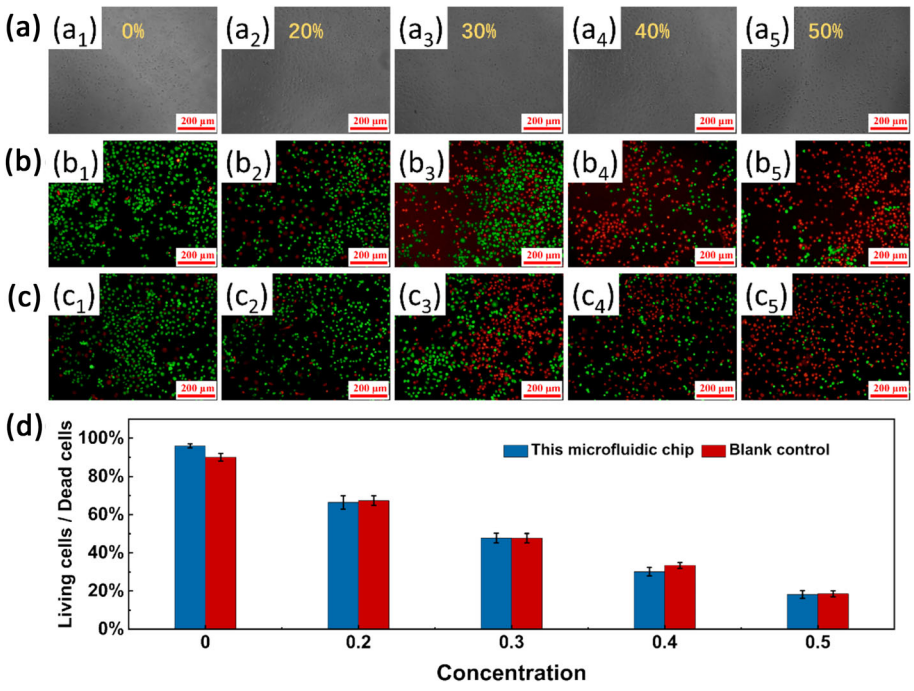

Fig. 7 The endothelial cells were stimulated by generating concentrations of adriamycin hydrochloride (20%–50%). **a** The endothelial cells were stimulated after 12 h. The scale bars denote 200 μm. **b** Generating concentration gradients (20%–50%) from the designed microfluidic chip. The scale bars denote 200 μm. **c** Blank control (taking the same concentration gradient through pipetting device configuration, corresponding to the microfluidic chip). The scale bars denote 200 μm. **d** Living cells/dead cells with concentration gradients

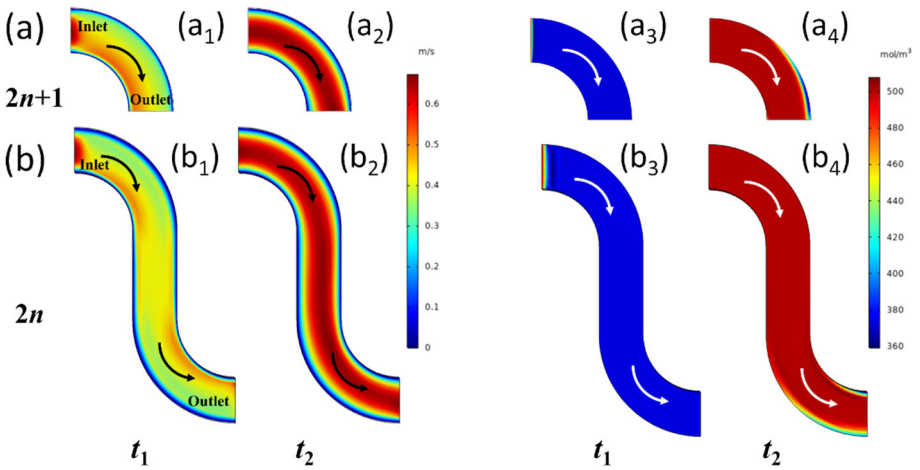

Fig. 8 The numerical results for velocity and concentration distribution in a microfluidic network with different numbers of L-junctions. $\mathbf{a_1}$ Odd number ($2n$+1), at t_1=0 s, velocity field. $\mathbf{a_2}$ Odd number ($2n$+1), at t_2=0.01 s, velocity field. $\mathbf{a_3}$ Odd number ($2n$+1), at t_1=0 s, concentration field. $\mathbf{a_4}$ Odd number ($2n$+1), at t_2=0.01 s, concentration field. $\mathbf{b_1}$ Even number ($2n$), at t_1=0 s, velocity field. $\mathbf{b_2}$ Even number ($2n$), at t_2=0.01 s, velocity field. $\mathbf{b_3}$ Even number ($2n$), at t_1=0 s, concentration field. $\mathbf{b_4}$ Even number ($2n$), at t_2=0.01 s, concentration field

Conclusions

In microfluidics, junction resistances cannot be ignored in the process of design. In this study, we demonstrate the importance of junctions through three examples. Besides the resistances along the straight path of rectangular, square, and round cross sections, we heavily focus on junction resistances of L-junctions, T-junctions, snaked junctions, and helix junctions. Through three cases including single-cell analysis, concentration gradient, and averaging control, we demonstrate that junction resistance matters for high precision microfluidics design. Importantly, this design method will be helpful to develop modular microfluidic systems that require precise characterization of each channel module. Compared with other design methods, ours provides a more accurate result because it fully considers junction resistance, and we also give a more convenient way to use the design method. This method can provide design parameters that facilitate the design of microfluidic networks. It may also

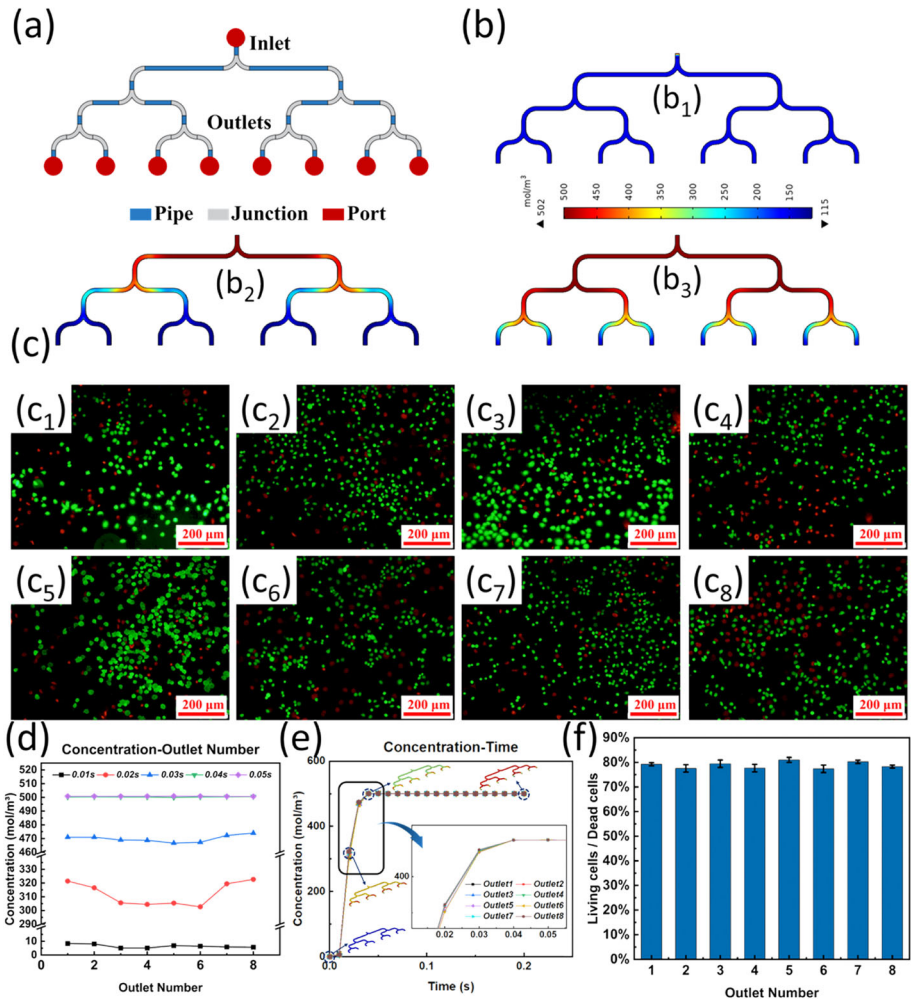

Fig. 9 Averaging concentration microfluidic network. **a** Schematic diagram. **b** The numerical result of the vertical view (*X*–*Y*) of the network. $\mathbf{b_1}$ *t*=0 s. $\mathbf{b_2}$ *t*=0.01 s. $\mathbf{b_3}$ *t*=0.02 s. **c** The endothelial cells were stimulated by generating concentrations of adriamycin hydrochloride. The scale bars denote 200 μm. $\mathbf{c_1}$ Outlet1. $\mathbf{c_2}$ Outlet2. $\mathbf{c_3}$ Outlet3. $\mathbf{c_4}$ Outlet4. $\mathbf{c_5}$ Outlet5. $\mathbf{c_6}$ Outlet6. $\mathbf{c_7}$ Outlet7. $\mathbf{c_8}$ Outlet8. **d** Concentration vs outlets at different times. **e** Concentration vs time at different outlets. **f** Living cell numbers vs dead cell numbers in different outlets

contribute to providing a platform for the precise design of organ chips.

Supplementary Information The online version contains supplementary material available at https://doi.org/10.1007/s42242-022-00215-1.

Acknowledgements This work was supported by the National Natural Science Foundation of China (Nos. 31970754 and 82072018) and the Strategic Priority Research Program (C) of the CAS (XDC07040200).

Author contributions YL and DLH developed the methodology of design and created models. ZRW and YRY made data curation. SW and GZS edited the paper. XYL assisted the implementation of the computer code and programming. ZHZ and YHQ supplied experimental assistance. PW supported the fruitful discussions. LQH and WPD planned the work.

Declarations

Conflict of interest The authors declare that they have no conflict of interest.

Ethical approval This article does not contain any studies with human or animal subjects performed by any of the authors.

Data availability The data supporting the results in this study are available within the paper and its supplementary information.

References

1. Whitesides GM (2006) The origins and the future of microfluidics. Nature 442(7101):368–373. https://doi.org/10.1038/nature05058
2. Dai L, Zhao X, Guo J et al (2020) Microfluidics-based microwave sensor. Sens Actuat A Phys 309:111910. https://doi.org/10.1016/j.sna.2020.111910
3. She X, Wang X, Niu P et al (2022) Miniature sono-electrochemical platform enabling effective and gentle electrode biofouling removal for continuous sweat measurements. Chem Eng J 431:133354. https://doi.org/10.1016/j.cej.2021.133354
4. Yu Y, Guo J, Ma B et al (2020) Liquid metal-integrated ultra-elastic conductive microfibers from microfluidics for wearable electronics. Sci Bull 65(20):1752–1759. https://doi.org/10.1016/j.scib.2020.06.002
5. Guo J, Yu Y, Zhang D et al (2021) Morphological hydrogel microfibers with MXene encapsulation for electronic skin. Research 2021:7065907. https://doi.org/10.34133/2021/7065907
6. Zilionis R, Nainys J, Veres A et al (2017) Single-cell barcoding and sequencing using droplet microfluidics. Nat Protoc 12(1):44–73. https://doi.org/10.1038/nprot.2016.154

7. Hindson BJ, Ness KD, Masquelier DA et al (2011) High-throughput droplet digital PCR system for absolute quantitation of DNA copy number. Anal Chem 83(22):8604–8610. https://doi.org/10.1021/ac202028g
8. Liu Y, Cheng Y, Zhao C et al (2022) Nanomotor-derived porous biomedical particles from droplet microfluidics. Adv Sci 9(4):e2104272. https://doi.org/10.1002/advs.202104272
9. Cai L, Chen G, Wang Y et al (2021) Boston ivy-inspired disc-like adhesive microparticles for drug delivery. Research 2021:9895674. https://doi.org/10.34133/2021/9895674
10. Fraser LA, Cheung YW, Kinghorn AB et al (2019) Microfluidic technology for nucleic acid aptamer evolution and application. Adv Biosyst 3(5):1900012. https://doi.org/10.1002/adbi.201900012
11. Bhatia SN, Ingber DE (2014) Microfluidic organs-on-chips. Nat Biotechnol 32(8):760–772. https://doi.org/10.1038/nbt.2989
12. Chu LY, Wan W (2017) Microfluidics for advanced functional polymeric materials (1st Ed.), Wiley-VCH. https://doi.org/10.1002/9783527803637
13. Damiri HS, Bardaweel HK (2015) Numerical design and optimization of hydraulic resistance and wall shear stress inside pressure-driven microfluidic networks. Lab Chip 15(21):4187–4196. https://doi.org/10.1039/c5lc00578g
14. Salva ML, Temiz Y, Rocca M et al (2019) Programmable hydraulic resistor for microfluidic chips using electrogate arrays. Sci Rep 9:17242. https://doi.org/10.1038/s41598-019-53885-w
15. Wang JC, Brisk P, Grover WH (2016) Random design of microfluidics. Lab Chip 16(21):4212–4219. https://doi.org/10.1039/c6lc00758a
16. Wang J, Zhang N, Chen J et al (2019) Finding the optimal design of a passive microfluidic mixer. Lab Chip 19(21):3618–3627. https://doi.org/10.1039/c9lc00546c
17. Wang J, Zhang N, Chen J et al (2021) Predicting the fluid behavior of random microfluidic mixers using convolutional neural networks. Lab Chip 21(2):296–309. https://doi.org/10.1039/d0lc01158d
18. Sanka R, Lippai J, Samarasekera D et al (2019) 3DμF - interactive design environment for continuous flow microfluidic devices. Sci Rep 9(1):9166. https://doi.org/10.1038/s41598-019-45623-z
19. Parker RW, Wilson DJ, Mace CR (2020) Open software platform for automated analysis of paper-based microfluidic devices. Sci Rep 10(1):11284. https://doi.org/10.1038/s41598-020-67639-6
20. Lashkaripour A, Rodriguez C, Mehdipour N et al (2021) Machine learning enables design automation of microfluidic flow-focusing droplet generation. Nat Commun 12(1):25. https://doi.org/10.1038/s41467-020-20284-z
21. Tanev G (2017) A correct-by-construction design and programming approach for open paper-based digital microfluidics. In: Symposium on design, test, integration and packaging of MEMS/MOEMS. https://doi.org/10.1109/dtip.2017.7984476
22. Gleichmann N, Malsch D, Horbert P et al (2014) Toward microfluidic design automation: a new system simulation toolkit for the in silico evaluation of droplet-based lab-on-a-chip systems. Microfluid Nanofluid 18(5–6):1095–1105. https://doi.org/10.1007/s10404-014-1502-z
23. Oh KW, Lee K, Ahn B et al (2012) Design of pressure-driven microfluidic networks using electric circuit analogy. Lab Chip 12(3):515–545. https://doi.org/10.1039/c2lc20799k
24. Cornish RJ (1928) Flow in a pipe of rectangular gross-section. Proc R Soc Lond 120(786):691–700. https://doi.org/10.1098/rspa.1928.0175
25. Choi S, Lee MG, Park JK (2010) Microfluidic parallel circuit for measurement of hydraulic resistance. Biomicrofluidics 4(3):034110. https://doi.org/10.1063/1.3486609
26. Vanapalli SA, Banpurkar AG, van den Ende D et al (2009) Hydrodynamic resistance of single confined moving drops in rectangular microchannels. Lab Chip 9(7):982–990. https://doi.org/10.1039/b815002h
27. Miguel AF (2010) Dendritic structures for fluid flow: laminar, turbulent and constructal design. J Fluids Struct 26(2):330–335. https://doi.org/10.1016/j.jfluidstructs.2009.11.004
28. Miguel AF (2018) A general model for optimal branching of fluidic networks. Phys A Stat Mech Appl 512:665–674. https://doi.org/10.1016/j.physa.2018.07.054
29. Razavi MS, Shirani E (2013) Development of a general method for designing microvascular networks using distribution of wall shear stress. J Biomech 46(13):2303–2309. https://doi.org/10.1016/j.jbiomech.2013.06.005
30. Reyes DR, van Heeren H, Guha S et al (2021) Accelerating innovation and commercialization through standardization of microfluidic-based medical devices. Lab Chip 21(1):9–21. https://doi.org/10.1039/d0lc00963f
31. Sayed Razavi M, Shirani E (2013) Development of a general method for designing microvascular networks using distribution of wall shear stress. J Biomech 46(13):2303–2309. https://doi.org/10.1016/j.jbiomech.2013.06.005
32. Li L, Wu P, Luo Z et al (2019) Dean flow assisted single cell and bead encapsulation for high performance single cell expression profiling. ACS Sens 4(5):1299–1305. https://doi.org/10.1021/acssensors.9b00171
33. Schmandt B, Herwig H (2015) The head change coefficient for branched flows: why "losses" due to junctions can be negative. Int J Heat Fluid Flow 54:268–275. https://doi.org/10.1016/j.ijheatfluidflow.2015.06.004
34. Schmandt B, Herwig H (2013) Performance evaluation of the flow in micro junctions: head change versus head loss coefficients. ASME 11th Internatinoal Conference on Nanochannels, Microchannels, and Minichannels. https://doi.org/10.1115/icnmm2013-73031
35. Schmandt B, Iyer V, Herwig H (2014) Determination of head change coefficients for dividing and combining junctions: a method based on the second law of thermodynamics. Chem Eng Sci 111:191–202. https://doi.org/10.1016/j.ces.2014.02.035
36. Bhargava KC, Thompson B, Malmstadt N (2014) Discrete elements for 3D microfluidics. Proc Natl Acad Sci USA 111(42):15013–15018. https://doi.org/10.1073/pnas.1414764111
37. Dai B, Long Y, Wu J et al (2021) Generation of flow and droplets with an ultra-long-range linear concentration gradient. Lab Chip 21(22):4390–4400. https://doi.org/10.1039/d1lc00749a
38. Tseng TM, Li M, Zhang Y et al (2019) Cloud Columba: accessible design automation platform for production and inspiration. IEEE/ACM International Conference on Computer-Aided Design. https://doi.org/10.1109/iccad45719.2019.8942104
39. Biral A (2013) Microfluidic networking: modelling and analysis. MS Thesis, Università degli Studi di Padova
40. Delplace F (2018) Laminar flow of newtonian liquids in ducts of rectangular cross-section an interesting model for both physics and mathematics. Int J Theor Math Phys 8(2):4. https://doi.org/10.15406/oajmtp.2018.01.00034
41. Zhuang QC, Ning RZ, Ma Y et al (2016) Recent developments in microfluidic chip for in vitro cell-based research. Chin J Anal Chem 44(4):522–532. https://doi.org/10.1016/s1872-2040(16)60919-2
42. Fu H, Liu X, Li S (2017) Mixing indexes considering the combination of mean and dispersion information from intensity images for the performance estimation of micromixing. RSC Adv 7(18):10906–10914. https://doi.org/10.1039/c6ra23783e

43. Lee CY, Chang CL, Wang YN et al (2011) Microfluidic mixing: a review. Int J Mol Sci 12(5):3263–3287. https://doi.org/10.3390/ijms12053263
44. Mahmud F, Tamrin KF (2020) Method for determining mixing index in microfluidics by RGB color model. Asia-Pac J Chem Eng 15(2):e2407. https://doi.org/10.1002/apj.2407